2013 13th IEEE-RAS International Conference on
Humanoid Robots (Humanoids).
October 15 - 17, 2013. Atlanta, GA

Anthrob – A Printed Anthropomimetic Robot

Michael Jäntsch[†,*], Steffen Wittmeier[†,*], Konstantinos Dalamagkidis[*], Alexander Panos[**], Fabian Volkart[**] and Alois Knoll[*]
[†]*The authors assert equal contribution and joint first authorship.*

***Abstract*— Anthropomimetic robotics differ from conventional approaches by capitalizing on the replication of the inner structures of the human body, such as muscles, tendons, bones and joints [1]. Prominent examples for this class of robots are the robots developed at the JSK laboratory of the University of Tokyo and the robots developed by the EU-funded project Embodied Cognition in a Compliantly Engineered Robot (Eccerobot). However, the high complexity of these robots as well as their lack of sensors has so far failed to provide the desired new insights in the field of control.**

Therefore, we developed the simplified but sensorized robot Anthrob. The robot replicates the human upper limb and features 13 compliant tendon driven uni- and biarticular muscles as well as a spherical shoulder joint. Whenever possible, Selective Laser Sintering (SLS) was used for the production of the robot parts to reduce the production costs and to implement cutting-edge technologies, such as tendon canals or solid-state joints.

***Keywords*—tendon-driven robots, anthropomimetic robots, biomechanics, biorobotics**

I. Introduction

In the past decade there was an increased interest in human-friendly robots, especially in the areas of service or rehabilitation robotics, where a possible impact can cause severe injuries or even death [2] Currently, three approaches are used to reduce these risks. These are (i) to employ additional sensors to *anticipate* impacts, (ii) to use more complex control strategies, such as joint torque control, to reduce the severity of inevitable collisions [3] or (iii) to exploit the concept of compliant tendon-driven actuation by imitating the human muscular system.

Particularly the tendon-driven approach has become increasingly popular in the past decade and a subclass of highly complex, tendon-driven robots has emerged. This subclass replicates the human skeletal and muscular system with an unprecedented level of detail and are therefore sometimes referred to as *musculoskeletal* or *anthropomimetic* robots [5]. Prominent examples for this class of robots are the robots Kenta, Kotaro, Kojiro [6], Kenzoh and Kenshiro [7] built by the Jouhou System Kougaku Laboratory of the University of Tokyo (JSK) since 2002 and the ECCEs developed by the EU-funded project Eccerobot between 2009 and 2012 [1]. However, even though these robots are extremely impressive artifacts, provably stable control strategies have so far not been developed. The reasons for this are manifold. First, the high complexity of the skeletal structures and the lack of suitable sensors (e.g. position sensors for spherical joints) renders the tracking of the robot dynamics and therefore the development of classical feedback controllers impossible. Furthermore, advanced control approaches rely on accurate dynamic models to compute feed-forward compensations of the non-linear dynamics. But this is only possible if an accurate model of the robot can be derived—a prerequisite which at least cannot be satisfied by the hand-crafted ECCEs. Therefore, we developed the simplified but sensorized anthropomimetic robot Anthrob (see Fig. 1). It replicates the human upper limb (shoulder girdle, upper arm and forearm) but includes some design simplifications in order to simplify the development of controllers without compromising key structures of anthropomimetic robots, namely spherical joints and multi-articular muscles. All skeletal parts of the robot are constructed using Computer-aided design (CAD) techniques to provide the required input data for the controller development and to facilitate the (re-)production of the robot. Furthermore, whenever possible, 3D printing technologies

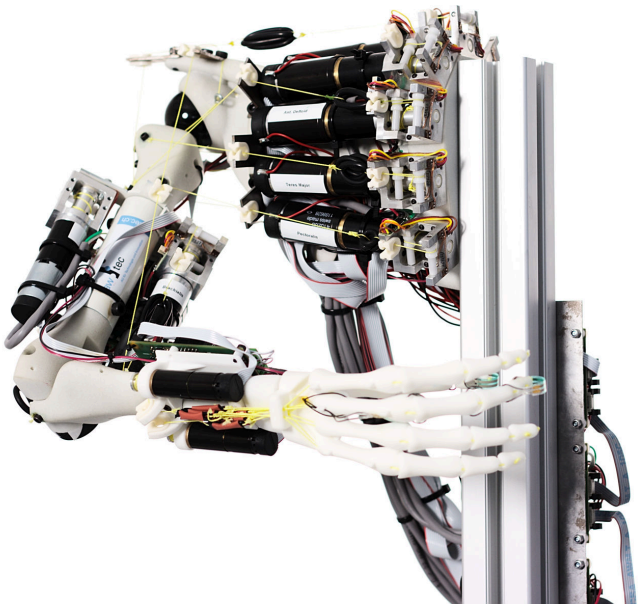

Fig. 1: Photograph of the developed anthropomimetic robot Anthrob. The robot replicates the human upper limb (upper arm, forearm and hand) and features 13 compliant tendon-driven muscles.

[*]These authors are with the chair for Robotics and Embedded Systems, Department of Informatics, Technische Universität München, Munich
[**]These authors are with awtec AG for technology and innovation, Zurich, Switzerland

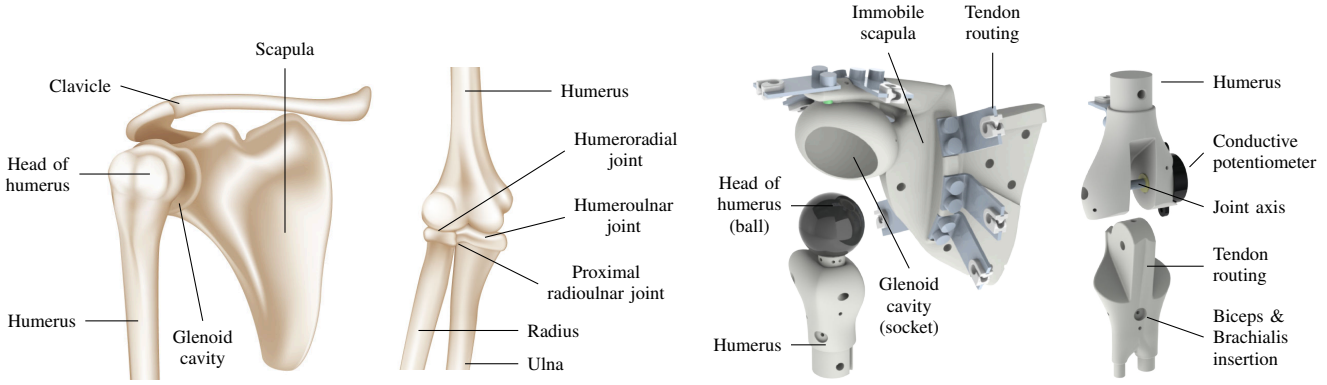

Fig. 2: Human and Anthrob shoulder and elbow joint. (a, b) Human shoulder and elbow joint (adapted from [4]). (c, d) Anthrob shoulder and elbow joint.

based on SLS have been used for the production of the robot parts to implement cutting-edge technologies, such as tendon canals or solid-state joints, and to minimize the production costs.

The robot kinematics (skeleton), actuators (muscles) and sensors (receptors) are summarized in section II. Preliminary results of robot motions, emerging from the utilization of low-level muscle controllers, are presented in section III, followed by conclusions in section IV.

II. The Design

The robot replicates the human upper limb, which comprises the bones of the pectoral girdle, the (upper) arm, the forearm and the hand [4]. It approximately has the size of 2/3 of a human male with height $1.70\,\mathrm{m}$, which yields an arm and forearm length of $200\,\mathrm{mm}$ and $180\,\mathrm{mm}$, respectively. Furthermore, the robot skeleton and muscles are designed to be capable of lifting and holding an interaction object with mass $500\,\mathrm{g}$ at the end-effector independent of the posture.

A. Skeleton

The shoulder complex can be considered as one of the most complicated human skeletal structures. It consists of the shoulder joint and the pectoral girdle. Whereas the spherical shoulder joint enables the movement of the humerus with respect to the scapula in three mutually perpendicular axes (see Fig. 2a), the pectoral girdle has two functions. First, it allows for scapula movements such as scapular elevation or depression [4]. Second, it extends the range of humerus movements [8] (e.g. during an abduction of the arm of more than $90°$). However, to reduce the complexity of the robot kinematics, only the shoulder joint was replicated. It consists of: (i) an immobile scapula, (ii) a glenoid cavity (or socket) and (iii) the humerus head (or ball) (see Fig. 2c).

In humans, the elbow joint is a compound joint comprising: (i) the humeroradial joint (a spherical joint between the humerus and the head of the radius), (ii) the humeroulnar joint (a revolute joint connecting the humerus to the ulna) and (iii) the proximal radioulnar joint (a pivot joint between the radius and the ulnar) [8], [4] (see Fig. 2b). While the proximal radioulnar joint allows for pronation and supination (the rotation of the radius around the ulnar), both the humeroradial and the humeroulnar joint contribute to the flexion and extension of the forearm [8]. Again, simplifications were made during the robot construction to imitate this complex compound joint. First of all, the ulnar and radius of the forearm were implemented as a single bone, which reduced the set of possible movements of the elbow joint to flexion and extension. Secondly, the omission of the radius and ulnar rendered the proximal radio-ulnar as well as two degrees-of-freedom of the humeroradial joint useless. Therefore, the elbow joint was implemented as a standard revolute joint with a maximum movement range of about $135°$ as shown in Fig. 2d. This range is comparable to reported human data where the movement range is approximately $145°$ with slight variations between females and males [8].

Another extremely complex but versatile human skeletal structure is the hand. Anatomically, it consists of the phalanges and the carpal and metacarpal bones and is connected to the forearm via the distal radioulnar and the radiocarpal joint [4]. This complicated skeletal structure allows for four primary types of grip: (i) the pinch or precision grip, (ii) the power grip, (iii) the key grip and (iv) the hook grip [4]. However, for the purpose of investigating the performance of robot controllers during manipulation tasks, the power grip is sufficient which yielded some design simplifications. First, the distal radioulnar and radiocarpal joints as well as the corresponding muscles were omitted and the hand was connected to the forearm via a passive but adjustable joint. This way, the posture of the hand does not change during manipulations but, if required, can be altered to match the requirements of a specific experiment. Secondly, the midcarpal joints, the joints between the proximal and distal rows of carpal bones, as well as the carpometacarpal joints, the joints between the carpal and metacarpal bones, of the index, middle, ring and little finger were not required.

The developed robot hand is shown in Fig. 3. It includes the five metacarpals as well as the five digits with their

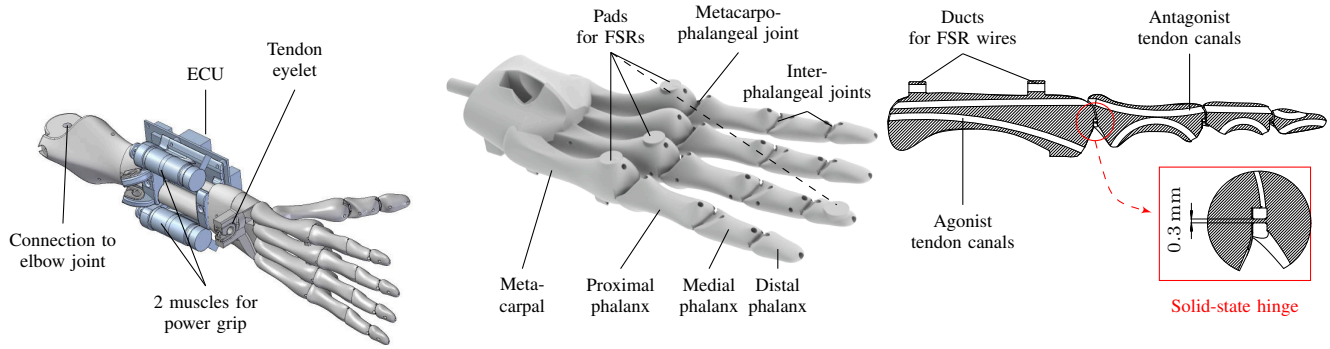

Fig. 3: Anthrob forearm and hand. (a) Anthrob forearm. The forearm is equipped with two muscle units to control the agonist and antagonist tendons of the hand. (b) Anthrob hand. The hand replicates the five metacarpals as well as the five digits of the human hand (thumb not shown). (c) Anthrob metacarpal and digit. Each metacarpal and digit features tendon canals for tendon routing as well as solid-state hinges for the metacarpophalangeal and interphalangeal joints.

proximal, medial and distal phalanges. The metacarpophalangeal as well as the interphalangeal joints are implemented as solid-state hinges. This was possible as the entire hand was produced by state-of-the art 3D printing technologies, namely SLS. In this type of joint, the movement of the two connected bones along the joint axis is enabled by a very thin film of material—here a $0.3\,\mathrm{mm}$ layer of Polyamid 2200 (PA-2200) (see Fig. 3c). Special care has to be taken that the material layers applied during the printing process are parallel to the desired joint axis, otherwise the joint will break. This approach not only resulted in a very slim and lightweight design but also made it possible to produce the hand from only two parts: (i) the thumb and (ii) the remaining four digits including the metacarpal and carpal bones. Moreover, due to the production technique, it was possible to include tendon canals and ducts for the wires of discriminative touch sensors (see Fig. 3c and subsection II-C), which further reduced the production costs and simplified the hand assembly.

B. Muscles

The human upper limb features more than 50 different muscles, of which some even constitute multiple heads. However, due to the skeletal simplifications made for the robot (see previous section), not all of these muscles need to be replicated in order to imitate human motions.

For instance, many muscles of the shoulder complex are required for scapula or clavicle movements. However, due to the omission of these bones, only the muscles that are concerned with humeral movements are important for the robot. Furthermore, some muscle heads, such as the long and short head of the biceps brachii, can be merged without loosing a significant range of upper arm movements. Therefore, the shoulder joint of the robot is actuated by nine muscles with origin and insertion points similar to their human analogous. However, it must be noted that human shoulder muscles often do not have a single origin and insertion point, but are linked to the bones via larger surfaces (e.g. Infraspinatus [4]). In

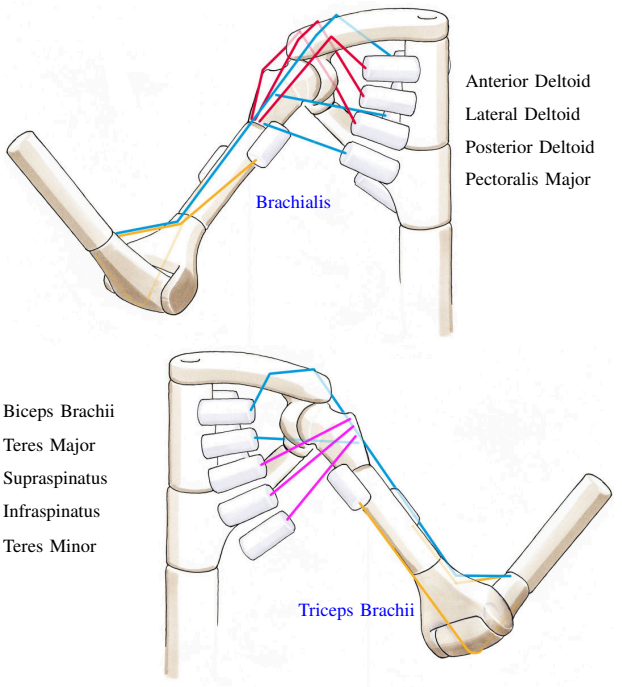

Fig. 4: Anthrob shoulder and elbow joint muscles and tendon routing (black labels: muscle unit type A, blue label: muscle unit type B, see Table I, illustrations by A. Jenter / awtec AG).

these cases, idealized muscle anchor points were chosen for the robot to imitate the function of their human counterpart (see Fig. 4, Table II, and [4]).

In humans, three muscles contribute to the elbow joint flexion and extension: (i) the brachialis, (ii) the triceps brachii, which has both uni- and biarticular heads, and (iii) the biceps brachii, which only has biarticular heads [4], [8]. For the robot, all three muscles were imitated, but only the biceps brachii was implemented as a biarticular muscle (see Table II). Again, the origin and insertion points were chosen

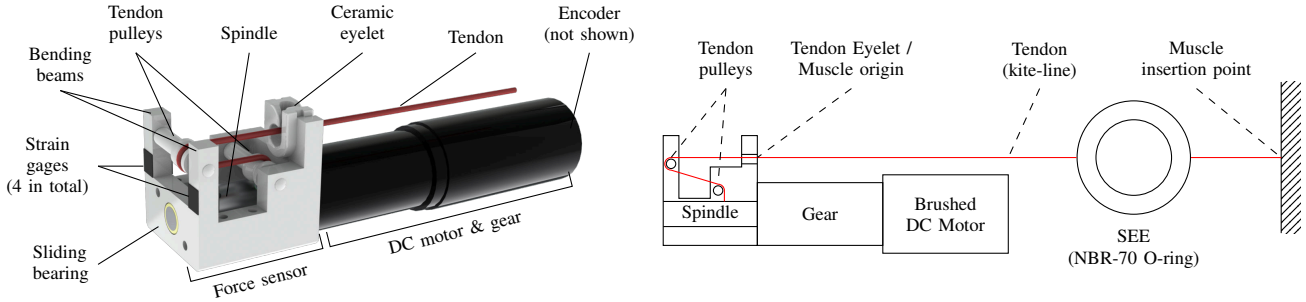

(a) (b)

Fig. 5: Anthrob muscle unit. Three sizes of muscle units have been developed for the Anthrob robot (see Table I). Each unit comprises a brushed DC motor, equipped with a gear, optional pulleys for tendon routing, sensors for muscle control and a spindle, supported by a sliding bearing. To imitate the viscoelastic properties of human muscles [9], each muscle additionally features an NBR O-ring as series elastic element (SEE). (a) Muscle unit rendering. (b) Muscle unit sketch.

TABLE I: Anthrob muscle unit types.

Muscle unit type	Actuator				Sensors	Tendon	
	ω_{nom} (rpm)	τ_{nom} (N m)	d_S (mm)	m (g)	Pos./ Force	d_T (mm)	f_{max} (N)
A	64.38	1.98	12	233	●/●	1	2000
B	33.38	0.63	12	170	●/●	1	2000
C	22.24	0.57	8	52	●/–	0.6	400

Legend: $\omega_{\text{nom}} \equiv$ nominal angular velocity, $\tau_{\text{nom}} \equiv$ nominal torque, $d_S \equiv$ spindle diameter, $m \equiv$ mass, $d_T \equiv$ tendon diameter, $f_{\text{max}} \equiv$ maximum tendon force

to imitate human muscle functions.

The implementation of the robot hand muscles significantly differs from the shoulder and elbow joint muscles. The main reason is that the targeted power grip does not require each digit to be controlled individually. Therefore, each digit was equipped with an agonist and antagonist tendon that are contracted simultaneously by two muscles—one for the agonist and one for the antagonist tendons of all digits (see Fig. 3c). However, to ensure that the hand adapts to the shape of the manipulated object during power grips, each of the 10 tendons featured a dedicated Nitrile butadiene rubber (NBR) ring as Series Elastic Element (SEE) (see Table II).

A modular muscle unit, based on the principle of series elastic actuator [10], has been developed for the muscles of the Anthrob robot. The muscle unit comprises a brushed Direct Current (DC) motor, equipped with a gear, optional pulleys for tendon routing, sensors for muscle control (see below) and a spindle which is supported by a sliding bearing to reduce radial forces on the transmission shaft. As tendon, two types of high-performance cords, made from braided ultra high molecular weight Polyethylene, were used (see Table I) and each muscle was equipped with an NBR O-ring as SEE to mimic the viscoelastic characteristics of human muscles (see [9] and Fig. 5b). NBR, which is a compound rubber, was selected as it exhibits a linear viscoelastic response for strains below 2.0 as observed by the experimental identification of the tensile properties of six different NBR O-ring types with varying inner and cross-section diameters (see Fig. 6). The viscoelastic response is characterized by a linear stress/strain relationship and a stress relaxation behavior (a decrease in the stress as response to an applied constant strain) reminiscent of the human muscle-tendon unit [9]. To match the force and stiffness requirements of the individual muscles, appropriate ring configurations were selected for each muscle based on the experimental results (see Table II). Similar to the muscle units used in other musculoskeletal robots, the muscle is contracted by coiling the tendon on the motor spindle [1], [7]. Therefore, the maximum linear velocity and force applied by the tendon depend on the spindle radius as well as on the maximum velocity and torque of the gear output shaft which in turn is defined by the used actuator (DC motor and gear). Here, three different combinations are used to match the specific force requirements of the shoulder joint, elbow joint and hand muscles (type A, B and C, respectively—see Table I and Table II). The combinations were selected by computing the worst-case tendon forces—minimal lever arms and maximum gravitational forces—of the shoulder, elbow and hand muscles during the interaction with an object weighing 500 g. A safety factor of 1.5 was considered to accomodate for the tendon friction forces due to the tendon routing.

C. Receptors

In humans, sensing "arises from a variety of receptors distributed throughout the body" [11]. In robotics, particularly the receptors that contribute to proprioception ("the sense of static positions and movements of the limbs of the body" [11]) and to discriminative touch (the sensing and localization of touch) are important for control and object manipulation. Therefore, the robot has been equipped with a variety of sensors to imitate these receptors.

In humans, three types of muscle and joint mechanoreceptors provide proprioceptive feedback: (i) the muscle spindle receptors which provide muscle length, velocity and stretch

feedback, (ii) the Golgi tendon organs that sense contractile forces exerted by a group of muscle fibers and (iii) the joint capsule mechanoreceptors that provide information about the current joint position [11]. Sensors to imitate these mechanoreceptors have also been included in the Anthrob robot. First of all, all muscle units were equipped with an encoder to measure the motor position and velocity and a Hall-effect-based motor current sensor, integrated in the Electronic Control Units (ECUs). Even though it is possible to estimate the output torque of a DC motor and therefore the tendon force from the current, this technique produces only reliable data for higher torques or at higher velocities, due to the friction losses in the gearbox. Therefore, all muscles of the shoulder and elbow joint (muscle unit type A and B, respectively) featured an additional custom-built tendon force sensor (see Fig. 5) which facilitated the implementation of a state-space tendon force controller. This sensor uses four strain gages, that are attached to either side of the two bending beams and that constitute a Wheatstone bridge, to measure the bending beam deflection and hence the applied tendon force. Moreover, to imitate the joint mechanoreceptors, the elbow joint was equipped with a conductive potentiometer. Unfortunately, similar sensors for the spherical shoulder joint are not available and optical substitutes are commonly used. Urata et al., for instance, developed a spherical joint sensor based on a micro camera integrated in the joint for the musculoskeletal robot Kotaro [12]. However, this sensor is not commercially available. Therefore, we developed a high-speed, stereo-vision motion capture system that uses infrared light and retroreflective markers, mounted to the scapula and humerus of the robot (not shown in Fig. 1) to track the joint position and velocity of the shoulder joint (see [13]). In human, the density of discriminative receptors is the "greatest on the hairless (glabrous) skin on the fingers, the palmar surface of the hand, the sole of the foot and the lips" [11]. Obviously, for object manipulation and identification, the finger and palmar surface receptors are particularly important. Therefore, the distal phalanx of the ring finger as well as three metacarpal heads of the robot hand were equipped with Force-sensitive Resistors (FSRs) to measure the grip force during manipulation (see Fig. 3b). To maximize the FSR sensitivity and improve the friction between the finger tip and the grabbed object, the thin material of the sensor itself was embedded between two layers of rubber material.

III. Results

All muscle units are controlled by distributed, custom-built Electronic Control Units (ECUs) which are interfaced via a Controller Area Network (CAN) [14], [1]. Each ECU is capable of controlling two muscle units and is equipped with a microcontroller, a CAN interface, motor drivers for two brushed DC motors, several Analog/Digital (A/D) converters for analog sensor connection and two integrated Hall-effect-based measurement devices in the motor loop for motor current feedback (see also subsection II-C). To achieve a high degree of robustness during robot operation, each ECU was implemented as a fail-silent unit with a firmware based on a Finite State Machine (FSM).

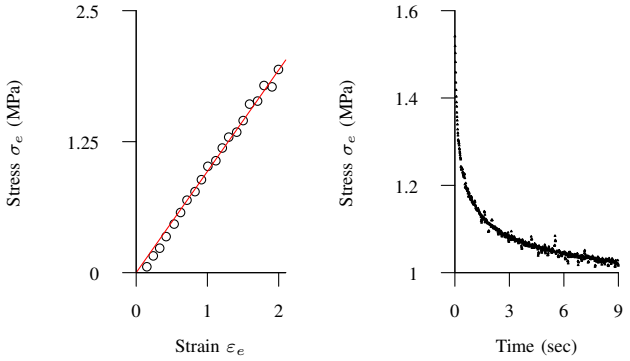

Fig. 6: Viscoelastic properties of an NBR O-ring with an inner and cross-section diameter of 10 and 5 mm, respectively. The ring exhibits a linear engineeering stress σ_e vs. strain ε_e relationship in the analyzed strain range (left panel, σ_e averaged over the first 0.1 s after strain application) and a stress relaxation response to an applied constant strain (right panel, $\varepsilon_e = 1.5$).

TABLE II: Properties of Anthrob muscles.

Muscle	X-articular	Muscle Unit Type	SEE l (mm)	SEE d (mm)	Quantity
Anterior Deltoid	uni	A	15	5	2
Lateral Deltoid	uni	A	15	5	2
Posterior Deltoid	uni	A	15	5	2
Pectoralis Major	uni	A	12	5	2
Teres Major	uni	A	12	5	2
Teres Minor	uni	A	12	5	2
Supraspinatus	uni	A	12	5	2
Infraspinatus	uni	A	12	5	2
Biceps Brachii	bi	A	15	5	2
Triceps Brachii	uni	B	10	4	1
Brachialis	uni	B	15	4	1
Agonist	multi	C	15	1	1*
Antagonist	multi	C	15	1	1*

Legend: $l \equiv$ inner diameter, $d \equiv$ cross section diameter, *one for each of the five digit tendons

To facilitate the development of high-level joint- or operational space controllers, a set of four low-level muscle controllers was developed and implemented on the ECUs. These are (i) a voltage control mode, (ii) a proportional-derivative (PD) motor position control mode, (iii) a proportional-integral-derivative (PID) current control mode and (iv) a state-space muscle force controller, which has proven to be superior to conventional PD approaches [15]. All controllers are executed with a control frequency of 1 kHz, which is sufficient as the SEEs slow down the muscle dynamics.

An example of an elbow joint flexion and subsequent extension induced by the motor position control of the three

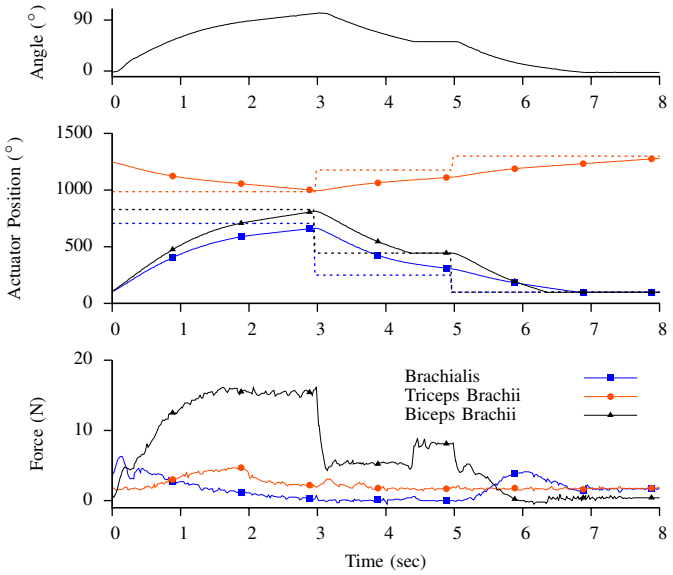

Fig. 7: Example of an elbow joint flexion and subsequent extension induced by the motor position control of the three elbow joint muscles (brachialis, triceps and biceps brachii, respectively). The figure shows the elbow angle (top panel), the reference (dashed) and current (solid) motor positions of all three muscles (center panel) and the corresponding muscle forces (bottom panel).

elbow joint muscles (brachialis, triceps and biceps brachii, respectively) is shown in Fig. 7. Here, new motor position references were set for all three muscles simultaneously at pre-defined times (e.g. at $t = 3\,\mathrm{s}$). However, even though the used control method is extremely simple, the observed elbow movements are smooth. This is an elegant example of Morphological Computation [16], as the compliant nature of the muscles compensates for timing inaccuracies and ensures that the forearm eventually reaches a steady-state. A compound movement of the entire upper limb of the robot can be observed in the attached video.

IV. Conclusions

We presented the design and implementation of the anthropomimetic robot Anthrob. The robot skeleton replicates the human upper limb and is produced mainly by 3D printing to reduce the production costs. Furthermore, special care was taken to faithfully reproduce the dynamics of the human muscular system. Here, tendon-driven, electromagnetic, and compliant muscles were developed that imitate the visco-elastic properties of human skeletal muscles. Moreover, in contrast to existing anthropomimetic robots, Anthrob was equipped with a large variety of sensors to mimic the receptors found in humans. Hence, a sensorized robotic platform was created that is capable of serving as a test bed for both neuroscientists and control engineers. This has already been demonstrated by the previously presented computed muscle control algorithm which was successfully evaluated on the robot [15]. However, we also hope that the application of this robot will not be limited to robotic applications per se but that it will ultimately help to shed new light on our understanding of human motion control.

V. Acknowledgments

The research leading to these results has received funding from the European Community's Seventh Framework Programme FP7/2007-2013 - Challenge 2 - Cognitive Systems, Interaction, Robotics - under grant agreement no. 231864 - ECCEROBOT.

References

[1] S. Wittmeier, C. Alessandro, N. Bascarevic, K. Dalamagkidis, D. Devereux, A. Diamond, M. Jäntsch, K. Jovanovic, R. Knight, H. G. Marques, P. Milosavljevic, B. Mitra, B. Svetozarevic, V. Potkonjak, R. Pfeifer, A. Knoll, and O. Holland, "Toward anthropomimetic robotics: Development, simulation, and control of a musculoskeletal torso," *Artificial Life*, vol. 19, no. 1, pp. 171–193, Nov. 2012.

[2] S. Haddadin, A. Albu-Schäffer, and G. Hirzinger, "Safety evaluation of physical human-robot interaction via crash-testing," in *Proceedings of Robotics: Science and Systems RSS*, 2007, pp. 217–224.

[3] A. Albu-Schäffer, O. Eiberger, M. Grebenstein, S. Haddadin, C. Ott, T. Wimbock, S. Wolf, and G. Hirzinger, "Soft robotics," *IEEE Robotics & Automation Magazine*, vol. 15, no. 3, pp. 20–30, 2008.

[4] M. Schünke, E. Schulte, L. Ross, U. Schumacher, and E. Lamperti, *Thieme Atlas of Anatomy: General Anatomy and Musculoskeletal System*, ser. Thieme Atlas of Anatomy Series. Thieme Medical Publishers, Incorporated, 2006, no. Bd. 433.

[5] O. Holland and R. Knight, "The anthropomimetic principle," in *Proceedings of the AISB06 Symposium on Biologically Inspired Robotics*, 2006.

[6] I. Mizuuchi, Y. Nakanishi, Y. Sodeyama, Y. Namiki, T. Nishino, N. Muramatsu, J. Urata, K. Hongo, T. Yoshikai, and M. Inaba, "An advanced musculoskeletal humanoid kojiro," in *Humanoid Robots, 2007 7th IEEE-RAS International Conference on*, 292007-dec.1 2007, pp. 294 –299.

[7] T. Kozuki, H. Mizoguchi, Y. Asano, M. Osada, T. Shirai, U. Junichi, Y. Nakanishi, K. Okada, and M. Inaba, "Design Methodology for the Thorax and Shoulder of Human Mimetic Musculoskeletal Humanoid Kenshiro – A Thorax structure with Rib like Surface," in *Proc. IEEE/RSJ International Conference on Intelligent Robots and Systems IROS*, 2012, pp. 3687–3692.

[8] W. Platzer and G. Spitzer, *Color Atlas of Human Anatomy: Locomotor System*, ser. Basic Sciences Series. Thieme Medical Publishers, Incorporated, 2009.

[9] D. C. Taylor, D. E. Brooks, and J. B. Ryan, "Viscoelastic characteristics of muscle: passive stretching versus muscular contractions," *Med Sci Sports Exerc*, vol. 29, no. 12, pp. 1619–1624, Dec 1997.

[10] G. A. Pratt and M. M. Williamson, "Series elastic actuators," in *Proc. IEEE/RSJ International Conference on Intelligent Robots and Systems IROS*, vol. 1, Aug. 1995, pp. 399–406.

[11] E. R. Kandel, J. H. Schwartz, and T. M. Jessel, *Principles of Neural Science*, 4th ed., J. Butler and H. Lebowitz, Eds. McGraw-Hill, 2000.

[12] J. Urata, Y. Nakanishi, A. Miyadera, I. Mizuuchi, T. Yoshikai, and M. Inaba, "A Three-Dimensional Angle Sensor for a Spherical Joint Using a Micro Camera," in *Proc. of the IEEE International Conference on Robotics and Automation*, 2006, pp. 4428–4430.

[13] S. Wittmeier, A. Gaschler, M. Jantsch, K. Dalamagkidis, and A. Knoll, "Calibration of a physics-based model of an anthropomimetic robot using evolution strategies," in *Intelligent Robots and Systems (IROS), 2012 IEEE/RSJ International Conference on*, oct. 2012, pp. 445 –450.

[14] M. Jäntsch, S. Wittmeier, and A. Knoll, "Distributed control for an anthropomimetic robot," in *Proc. IEEE/RSJ Int Intelligent Robots and Systems (IROS) Conf*, 2010, pp. 5466–5471.

[15] M. Jäntsch, S. Wittmeier, K. Dalamagkidis, and A. Knoll, "Computed Muscle Control for an Anthropomimetic Elbow Joint," in *Proc. IEEE/RSJ Int Intelligent Robots and Systems (IROS) Conf*, 2012.

[16] R. Pfeifer and G. Gómez, "Morphological Computation — Connecting Brain, Body, and Environment," in *Creating Brain-Like Intelligence*, ser. Lecture Notes in Computer Science. Springer Berlin / Heidelberg, 2009, vol. 5436, pp. 66–83.